Performance of the Hail Differential Reflectivity (H_{DR}) Polarimetric Radar Hail Indicator

TRACY K. DEPUE

Northrop Grumman Information Technology, Albuquerque, New Mexico

PATRICK C. KENNEDY AND STEVEN A. RUTLEDGE

Department of Atmospheric Science, Colorado State University, Fort Collins, Colorado

(Manuscript received 17 April 2006, in final form 12 December 2006)

ABSTRACT

A series of poststorm surveys were conducted in the wake of hailstorms observed by the Colorado State University–University of Chicago–Illinois State Water Survey (CSU-CHILL) S-Band polarimetric radar. Information on hail characteristics (maximum diameter, building damage, apparent hailstone density, etc.) was solicited from the general-public storm observers that were contacted during the surveys; the locations of their observations were determined using GPS equipment. Low-elevation angle radar measurements of reflectivity, differential reflectivity Z_{DR}, and linear depolarization ratio (LDR) were interpolated to the ground-observer locations. Relationships between the hail differential reflectivity parameter H_{DR} and the observer-reported hail characteristics were examined. It was found that H_{DR} thresholds of 21 and 30 dB were reasonably successful (critical success index values of ~0.77) in respectively identifying regions where large (>19 mm in diameter) and structurally damaging hail were observed. The LDR characteristics in the observed hail areas were also examined. Because of sensitivities to variations in the hailstone bulk ice density, degree of surface wetness, and shape irregularities, the basic correlation between LDR magnitude and hail diameter was poor. However, when the reported hail diameters exceeded ~25 mm, LDR levels below ~−24 dB were uncommon.

1. Introduction

Numerous imaging and theoretical studies have established that the net forces acting on falling raindrops with diameters larger than ~1 mm cause them to assume oblate shapes with their shortest axis generally oriented along the vertical direction (Pruppacher and Beard 1970; Beard and Chuang 1987). During the early stages of polarimetric meteorological radar research, it was recognized that this preferred drop orientation would cause the radar reflectivity observed at horizontal (H) polarization to be slightly greater than that observed at vertical (V) polarization (Seliga and Bringi 1976). This polarization-dependent reflectivity difference is expressed by the differential reflectivity Z_{DR}:

$$Z_{DR} = 10 \log_{10}(Z_{HH}/Z_{VV}), \quad (1)$$

where the first and second subscripts are the received and transmitted polarizations, respectively.

Thus, oblate raindrops will generate positive Z_{DR} values. In contrast to the preferred orientation characteristics of raindrops, the aerodynamic forces acting on falling moderate to large diameter hailstones typically cause them to undergo large amplitude (>~45°) gyrations (Knight and Knight 1970b). On average, these large orientation excursions tend to equalize Z_{HH} and Z_{VV}, causing the Z_{DR} value for such hailstones to be near 0 dB.

Aydin et al. (1986) developed the hail differential reflectivity (H_{DR}) parameter to distinguish hail from rain in Z_{HH}, Z_{DR} space (Fig. 1). Specifically,

$$\begin{aligned} H_{DR} &= Z_{HH} - f(Z_{DR}), \quad \text{where} \\ f(Z_{DR}) &= 27, (Z_{DR} \le 0 \text{ dB}), \\ &= 19Z_{DR} + 27, (0 \le Z_{DR} \le 1.74 \text{ dB}), \\ &= 60, (Z_{DR} > 1.74 \text{ dB}). \end{aligned} \quad (2)$$

Corresponding author address: Pat Kennedy, Dept. of Atmospheric Science, Colorado State University, Fort Collins, CO 80523.
E-mail: pat@lab.chill.colostate.edu

DOI: 10.1175/JAM2529.1

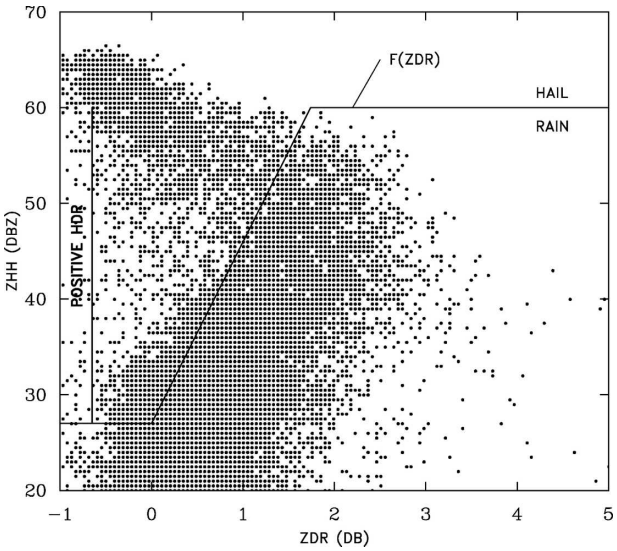

FIG. 1. Scatterplot of Z_{HH} and ZDR data collected by the CSU-CHILL radar at 0.5° elevation angle at 2343 UTC 6 Jun 2003. The H_{DR} rain–hail boundary as defined in Aydin et al. (1986) is included. (After Fig. 6 in Aydin et al. 1986.)

The resultant three line segments define the rain–hail boundary plotted in Fig. 1. The H_{DR} is positive for Z_{HH}, Z_{DR} pairs located vertically above the rain boundary, where the combination of relatively small Z_{DR} values with large Z_{HH} reflectivities is indicative of hail. Originally, H_{DR} was intended to provide a yes/no indication of the presence of hail; its capability to provide additional information on hail size, damage potential, etc., has received relatively little interest. Brandes and Vivekanandan (1998) found a positive correlation between H_{DR} magnitudes and observed hail diameter in two Colorado hailstorms. Mezzasalma et al. (2000) found only modest correlation between H_{DR} levels above 13 dB and the occurrence of impact impressions in a hail pad network in Italy. However, limitations in the spatial resolution of the hail pad network (one pad per 16 kilometers squared), the temporal resolution of the radar data (one Z_{DR} volume per 15 minutes), and the Z_{DR} uncertainties introduced by the effects of differential attenuation at C-band all impacted the results of their study. Thus, one goal of the research reported in this study is the examination of the correlation between S-band (11-cm wavelength) H_{DR} values and observed surface hail characteristics for a reasonably large number of storm events.

The second goal of the current research is to investigate possible associations between linear depolarization ratio (LDR) and observed hailstone characteristics. Here LDR is defined as

$$\mathrm{LDR} = 10 \log_{10}(Z_{VH}/Z_{HH}). \quad (3)$$

Qualitatively, the tumbling motions of nonspherical high-density hailstones should increase the cross-polarized component of the backscattered radar signal (Herzegh and Jameson 1992), thereby increasing LDR. Since there is some tendency for larger diameter hailstones to become increasingly nonspherical (Knight 1986), LDR measurements may provide additional information on hailstone diameters.

2. Microwave backscattering computations

a. Background

A numerical model of radar backscattering based on the transition matrix (**T** matrix) methods of Waterman (1965) was used to obtain a sense of the response of Z_{DR} and LDR to variations in the physical properties of hailstones. The modeling computations were done using a two-step procedure. The first step is the calculation of **T**-matrix values for each hailstone size of interest. In addition to diameter (for nonspherical particles, diameter corresponds to that of a spherical particle of equal volume), the axis ratio and bulk refractive index of the modeled particles are specified. The **T**-matrix calculations also allow the effects of a water film of specified thickness on the surface of the hailstone to be included. In the second modeling step, parameterizations of the particle concentrations and orientations are considered. The model then calculates the net backscatter radar signal by summing the basic particle-specific **T**-matrix scattering representations in accordance with the prescribed concentration and orientation information.

To make the scattering calculations practical, the physical properties describing the modeled hailstones ignored several of the complexities that are often characteristic of naturally occurring hailstones. The hailstone shapes are taken to be smoothly deformed spheroids. Other hailstone shapes (i.e., conical, triaxial forms, lobed external protrusions, etc.; Knight and Knight 1970a) were not considered. Water-coating thickness in the model remain constant across the surface of the hailstone even though wind tunnel studies have demonstrated that hailstone water coatings are typically redistributed by aerodynamic and rotation-related forces (Rasmussen and Heymsfield 1987). The uniform water-coating thickness used here (0.5 mm) approximates an average water-coating depth that would result if the water layer mass was uniformly distributed over the outer surface of a large (>19 mm in diameter) hailstone. Last, the modeled hailstone's refractive index value is taken to be uniform within the ice material, disregarding the known layered variations in ice structure, internal bubbles, etc. that normally are

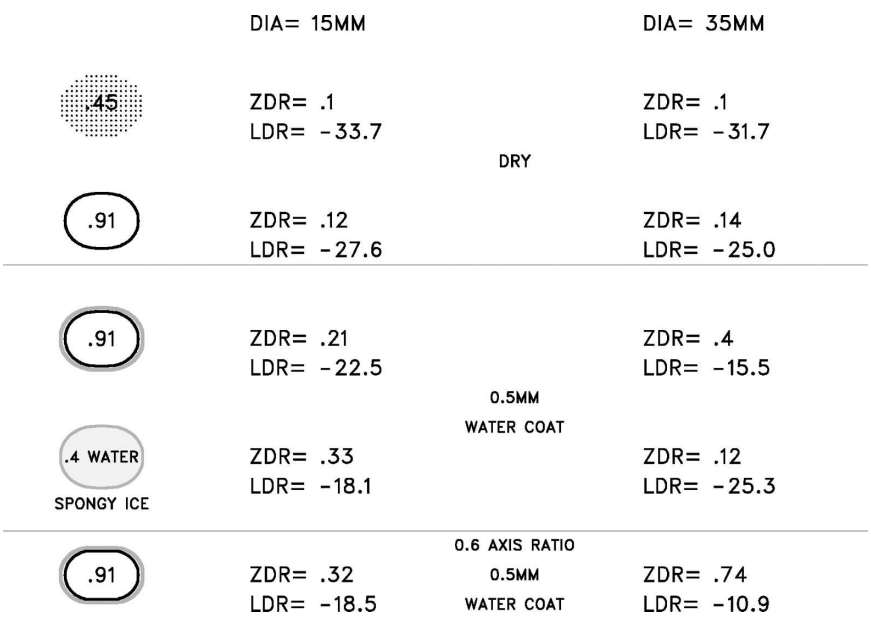

FIG. 2. The Z_{DR} and LDR values calculated by the **T**-matrix model for hailstone diameters of (center) 15- and (right) 35-mm diameter. Hailstone physical characteristics for each row are depicted in the left column: Except for the spongy ice case, decimal numbers in the center of the schematic hailstones are the ice bulk density in g cm^{-3}. In the spongy ice case, the value of 0.4 indicates that the hailstone dielectric properties are based on a mixture of 40% water and 60% ice. Gray horizontal lines separate the results for simulations for various water coating and axis ratio regimes. Hailstone axis ratio is 0.75 except for the bottom row where it is 0.6. In all cases, the canting angle distribution is Gaussian with a mean of 0° and a standard deviation of 75°.

observed in hailstone cross sections. Thus, the scattering model results should be regarded only approximations of the polarimetric signals observed from natural hailstones.

b. Monodisperse hailstone diameter distribution results

Selected scattering model results for hailstone diameters of 15 and 35 mm at an S-band (11 cm) wavelength are summarized in Fig. 2. [These two diameters bracket the National Weather Service large hail diameter threshold of 19 mm (0.75 in.).] Except for the bottom row in Fig. 2, all of the calculations are based a hailstone axis ratio of 0.75. In the bottom row, the axis ratio is 0.6. The orientation angle between the stone's minor axis and the vertical direction varies according to a Gaussian distribution with a mean of 0° and a standard deviation of 75°. While these hailstone shape and orientation values were subjectively selected, they are in general agreement with observed hail characteristics (Knight and Knight 1970b). The physical hailstone properties used in the various scattering model runs are indicated schematically along the left edge of the figure. The modeling results have been arranged so that hailstone composition varies from a low bulk density ice–air mixture in the first line of the figure through various combinations of water-coated and/or water-soaked (labeled as spongy) ice toward the bottom of the figure. In general, the magnitudes of the Z_{DR} and LDR values increase as the simulated hailstone composition becomes increasingly dense and wet. Also, resonance effects due to Mie scattering are apparent in the ~10-dB LDR variations that occur in the water-coated and water-soaked ice cases at the 35-mm diameter.

These basic scattering calculation results are extended across a range of hailstone diameters in Fig. 3. As in Fig. 2, the axis ratio has been fixed at 0.75. The curves depict several combinations of hail wetness and canting angle standard deviation. The resultant Z_{DR} responses are shown in Fig. 3a. The largest Z_{DR} fluctuations occur when the canting angle standard deviation is reduced to 25°. Under these conditions, the mean orientation of the hailstone's major axis remains much closer to the horizontal than to the vertical, yielding nominally positive Z_{DR} values. The resultant Z_{DR}s exceed 1 dB as the hail diameter reaches ~40 mm. Just beyond this point, additional diameter increases, causing Mie scattering effects that begin to reduce Z_{HH}

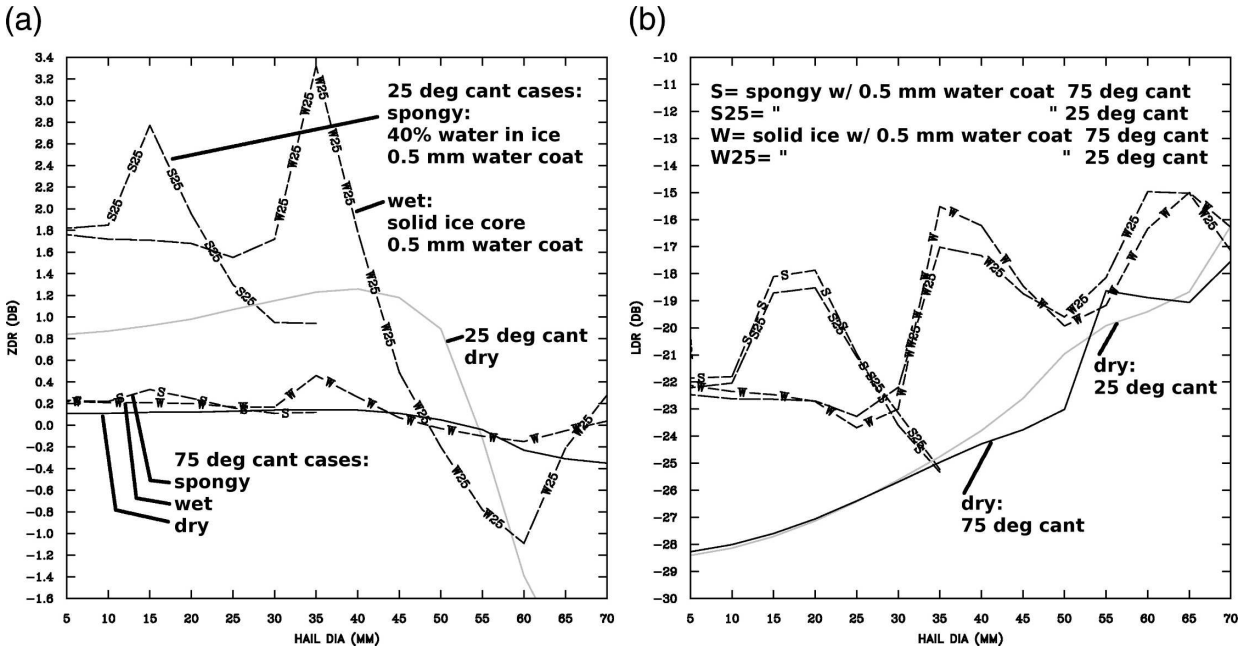

FIG. 3. (a) The Z_{DR} calculated by the **T**-matrix model as a function of hailstone diameter. Particle axis ratio is fixed at 0.75. Hailstone physical characteristics for each curve are marked; dry indicates 0.91 g cm^{-3} ice density with no outer water coating. Canting angle values refer to the standard deviation (°) specified for a Gaussian distribution of canting angles about a mean of 0°. (b) As in (a), but the curves are LDR.

more rapidly than Z_{VV}, producing distinctly negative Z_{DR} values as the diameter reaches 60 mm. This pattern of initially positive Z_{DR}s followed by a sharp Z_{DR} reduction with increasing hail diameter is magnified when water either coats the hailstone or when water becomes a major fraction of the stone's mass (in this study a water mass fraction of 40% is considered to be significant). The Mie resonance effects also appear at smaller diameters for the wet hail cases under the 25° canting angle standard deviation condition. In the second set of three curves plotted in Fig. 3a, the canting angle standard deviation is increased to 75°. Mie-induced Z_{DR} fluctuations appear in the two wet hail cases, but the magnitudes of these deviations are generally less than 0.5 dB. Thus, Z_{DR} fluctuations due to Mie resonance effects tend to decrease as the hailstone orientations become increasingly random.

Figure 3b shows the LDR values calculated for the same conditions that were used in Fig. 3a. The reduction of the canting angle standard deviation from 75° to 25° has comparatively little effect upon LDR for the dry hail cases with diameters under ~45 mm. In contrast, the introduction of an outer water coating and a liquid water component inside the hailstone ice structure (i.e., spongy ice) causes several dB LDR fluctuations to begin to appear at hail diameters as small as ~10–35 mm.

c. *Exponentially distributed hailstone diameter results*

Observations have demonstrated that an approximately exponential distribution of hailstone diameters typically is present in natural hailfalls (Hubbert et al. 1998; Cheng and English 1983). Thus, additional **T**-matrix scattering model runs were conducted to consider the effects of a population of hailstone diameters and shapes upon the computed radar quantities. In these model runs, exponential input size distributions between prescribed diameter limits were considered. The size distributions were given by

$$N(D) = N_0 e^{-\lambda D}, \tag{4}$$

where $N(D)$ is the volumetric concentration of hailstones within the D, D + dD diameter interval, D is the hail diameter, and N_0 and λ are the intercept and slope parameters respectively. The **T**-matrix model integrations were carried out starting from a fixed lower diameter limit of 3 mm. The upper integration limit was increased sequentially from 8 to 53 mm in 5-mm increments. According to Ulbrich and Atlas (1982), for typical hail size distributions, the product of the slope parameter and the maximum hail diameter is typically a relatively constant value. For the National Hail Research Project (i.e., northeastern Colorado) data pre-

TABLE 1. The **T**-matrix model results for exponential hail size distributions. Radar data values in each row are the result of integrating over a specified hail size spectrum from a diameter of 3 mm up to a diameter of D_{max}. Water-coating thickness is 0.5 mm.

D_{max} (mm)	dBZ	Z_{DR}	H_{DR}	LDR
53	73.8	0.0	46.8	−19.1
48	73.0	0.1	44.1	−19.3
43	71.1	0.2	41.1	−19.0
38	66.7	0.2	35.2	−19.9
33	62.3	0.2	30.7	−20.1
28	62.6	0.2	32.6	−24.1
23	61.8	0.2	31.4	−23.7
18	58.9	0.2	28.7	−24.5
13	53.0	0.1	23.6	−26.9
8	44.6	0.1	15.2	−26.8

sented in the appendix of Ulbrich and Atlas (1982), this constant is distributed between ~4 and 14 (diameter is in centimeters). For these model runs, the constant was set to the upper limit of the Ulbrich and Atlas (1982) range (i.e., $\lambda = 14/D_{max}$). The distribution intercept parameter was then defined using a modified version of the power-law relationship with λ proposed by Cheng and English (1983). The constants selected for use in these expressions were not designed to represent any unique hail size distribution; instead, they were only chosen so that reasonable reflectivity magnitudes were maintained as the upper integration diameter limit was varied.

At each hail diameter within the size distribution, the particle axis ratio used in the scattering calculations was taken from the data for northeast Colorado shown in Fig. 1 of Knight (1986). In accordance with this curve, the hailstone shapes became less spherical with increasing diameter (i.e., axis ratio of ~0.86 at 10-mm diameter and ~0.76 at 50-mm diameter). The hailstone spatial orientations followed a Gaussian distribution with a standard deviation of 75° about a mean of 0°. Last, the radar wavelength was fixed at 11 cm, the temperature was set at 0°, and the hailstone ice density was 0.91 g cm^{-3}.

Table 1 summarizes the results of these **T**-matrix simulations when the modeled hailstones had a uniform 0.5-mm-thick water coating. In a similar pattern to the single diameter results in Fig. 3a, the Z_{DR} values remain under 0.3 db for all of the simulated conditions. LDR generally increases as the larger, less spherically shaped hailstones are introduced at the larger diameter end of the spectrum. This basic trend is influenced by Mie resonance effects as evidenced by the 4-dB LDR jump when the maximum diameter increases from 28 to 33 mm. Table 2 presents similar results for dry hail (i.e., no water coating) case. No Z_{DR} variations are apparent in this case. The reflectivity and LDR magnitudes are both reduced by several decibels from the levels seen in the water-coated hail simulation. LDR values approaching −20 dB do not appear until the maximum diameter in the hail size distribution exceeds 50 mm.

TABLE 2. As in Table 1, but with no water coating.

D_{max} (mm)	dBZ	Z_{DR}	H_{DR}	LDR
53	63.9	0.1	35.5	−21.6
48	66.0	0.1	37.0	−24.5
43	67.4	0.1	38.3	−25.9
38	67.3	0.1	38.2	−27.0
33	66.0	0.1	36.2	−25.3
28	63.7	0.1	34.0	−25.5
23	60.5	0.1	31.3	−27.6
18	56.0	0.1	27.2	−29.5
13	48.9	0.1	20.6	−32.6
8	39.2	0.1	11.0	−33.0

Taken as a whole, the **T**-matrix model results confirm that Z_{DR} should remain fairly close to 0 dB for most of the observed hail stone sizes, compositions, and orientations. It should be noted that exceptions to this situation have been reported. Smyth et al. (1999) documented a hailstorm in which a preferential orientation of oblate hailstones yielded Z_{DR} values of ~3 dB. The model results conducted here also confirm that depolarization levels generally increase with increasing hail size. However, the nature of this correlation is strongly influenced by the existence of liquid water either on the outside of the hailstone's surface or within the ice structure.

3. Hail observations in relationship to polarimetric radar data

a. Ground surveys of hail areas

To assess the correlations between H_{DR}, LDR, and observed hail characteristics, a number of poststorm ground surveys were conducted as soon as possible after suspect hailstorms were observed by the CSU-CHILL radar. The CSU-CHILL radar is an S-band, dual polarization research radar based near Greeley, Colorado (Brunkow et al. 2000). When thunderstorms were expected, the nominal scan pattern executed by the CSU-CHILL radar consisted of a series of four low-elevation angle (0.5° to 2.5°) 360° plan position indicator (PPI) scans. These volumes continuously repeated at a cycle time of slightly over 4 min. During a few of the operations, the volume scan cycle time was further decreased through the use of sector scans.

To identify prospective storm survey areas, thunder-

TABLE 3. Storm date and data points summary. (Location names are in Colorado unless otherwise noted.)

Date	Name	No. data points
20 Jun 2001	Watkins	7
3 Jun 2002	Fort Morgan	14
3 Jun 2002	Brighton	13
3 Jun 2002	Hereford	2
15 Jun 2002	Grasslands	1
15 Jun 2002	Watkins	3
19 Jun 2002	Timnath	7
3 Jul 2002	Severance	4
3 Jul 2002	Hudson	8
10 Jul 2002	The Pinery	16
24 Aug 2002	Merino	8
24 Jun 2003	Hillsdale, WY	3

TABLE 4. CSU-CHILL radar operating characteristics during the H_{DR} project (SNR is signal-to-noise ratio).

Wavelength	11.01 cm
Antenna diameter	8.5 m
3-dB beamwidth	1.1°
Transmit power	~700 kW
Pulse duration	1 μs
PRF	960 Hz
Transmit polarization	Alternating H, V
Pulses per integration cycle	128 (64 H + 64 V)
Azimuth scan rate	6° s^{-1}
Receiver noise power	~−113 dBm (SNR = 1)

storm echoes observed in the 0.5° PPI scan data were visually examined for the existence of the high reflectivity/low Z_{DR} pattern associated with hail. Hail reports filed by National Weather Service severe weather spotters were also used to target the survey regions. Once a prospective survey region was identified, the general goal was to conduct a driving survey of the area during which interviews of people directly affected by the hail were conducted. To map the width of surface hail swaths and to sample spatial variations in hail characteristics, efforts were made to contact observers located along roads that crossed the storm tracks. To ensure that the data pertained to the storm under investigation, initial questions were asked to confirm the date and general time of the observations being recounted. The observers were then presented with a collection of spherical objects of various sizes, including wooden balls, glass marbles, and so on, from which they selected the object(s) that best approximated the largest hailstones that they saw. Since the observer's detailed appreciation of the hailstone axis ratios was probably very subjective, the reported diameters were taken to be the major diameters of the stones. The observers were also asked a standardized series of questions regarding their observations of hail-related damage to local vegetation, vehicles, and structures. Information on the softness of the hail, as evidenced by the stone breaking up upon ground impact, was also solicited. A hand-held GPS device was used to determine the observer's location. A spreadsheet database format was developed to organize and store the data obtained from the observers. (A summary of the storms for which postevent surveys were conducted is shown in Table 3.) In general, the information collected from the observers was necessarily subjective. (In a few instances, observers presented example hailstones that they had saved in their home freezers.) It is felt that their storm recollections, especially when multiple observations of the same storm formed spatially coherent hail size and damage patterns, were adequate for the purposes of this study.

b. Radar data analysis procedures

A Cressman (1959) weighting scheme was used to interpolate the individual range gate data collected by the CSU-CHILL radar to the GPS-determined observer locations. The signal processor output gate data at increments of 150 m in range and 0.8° in azimuth (Table 4). The radar data were obtained from the 0.5° PPI sweep unless excessive beam blockage, or signal contamination due to ground clutter, overlaying range-aliased echoes, and so on were present. In these cases, data from the lowest contamination-free elevation angle was used. The cutoff radius imposed in the interpolations generally approximated the beamwidth of the antenna pattern at the average range to the hail survey area. Typically the data from 6–12 range gates entered into each interpolation.

Several quality control thresholds were applied to the gate data prior to the interpolation step. To remove noise and nonconvective precipitation echoes, the correlation between the copolar H and V return signals at lag zero [$\rho_{HV}(0)$] was required to be greater than 0.85, and the basic Z_{HH} reflectivity was required to be at least 45 dBZ. Gates with radial velocity values typical of ground clutter targets were removed. (Specifically, the disallowed velocities had magnitudes less than 1.1 m s^{-1} or greater than 25.4 m s^{-1}. The high velocity threshold is due to the displacement of zero radial velocities to near-Nyquist values when the differential propagation phase shift upon scattering from ground targets exceeds 90° under alternating VH transmit polarization mode.) Additionally, gates with the excessively negative Z_{DR} values ($Z_{DR} < -1.25$ dB) observed from many ground clutter targets were also discarded. The generally isolated nature of the thunderstorms analyzed in this study resulted in relatively short (<~15

km) beam paths through heavy (>~50 dBZ) precipitation regions. No attenuation corrections were applied to the basic Z_{HH} and Z_{DR} values. (Such attenuation corrections become more critical in regions were large scale convective systems typically occur.) If the thresholding procedures left only a single acceptable gate within the limiting Cressman radius, the interpolation results were considered to be invalid. For each event, interpolated radar data values were generated at all of the ground observation locations as the storm transited the area. The scan yielding the most positive H_{DR} value at each interpolation point was identified. The radar measurements made during the peak H_{DR} scan were taken to represent the polarimetric radar values associated with the hail information reported by the ground observers; also, the observers tended to recall the most extreme portion of the storm passage.

Last, it was also recognized that when ground observers were located in the high reflectivity gradient regions near the edges of the thunderstorm echoes, radar measurement errors due to nonuniform beam filling and antenna beam pattern imperfections would be more likely. To reduce these errors, a procedure was developed to estimate the reflectivity gradients that existed when the peak H_{DR} occurred at each observation point. The two radials that enclosed the ground observer's GPS location in the maximum H_{DR} scan were identified and azimuthal and radial reflectivity gradients centered at the observer locations were calculated. All of the ground observation data points were entered into an azimuthal versus radial reflectivity gradient domain scatterplot. The observations noted by observers in high gradient portions of the scatterplots were checked for statements indicating that they were near the edges of the hail region (i.e., especially remarks about hailfalls consisting of a limited number of stones and/or very brief hailfall durations). Subjectively chosen reflectivity gradient limits of 15 dB $(^\circ)^{-1}$ in azimuth and 20 dB km^{-1} in range were found to remove the observations that seemed to most clearly come form the hailswath edge regions. The application of these reflectivity gradient limits removed 13 points from the ground observation database; a total of 86 hail reports from the poststorm interviews remained available for processing.

An example of a combination of the CSU-CHILL radar data and the poststorm hail survey results for the 3 June 2002 storm near Brighton, Colorado, is shown in Fig. 4. As the storm crossed the area of interest, Z_{HH} and Z_{DR} data from the 0.5° PPI angles in each volume scan were interpolated to a regularly spaced (0.75 km mesh) set of Cartesian grid points. The H_{DR} values were then calculated at each grid point. The maximum

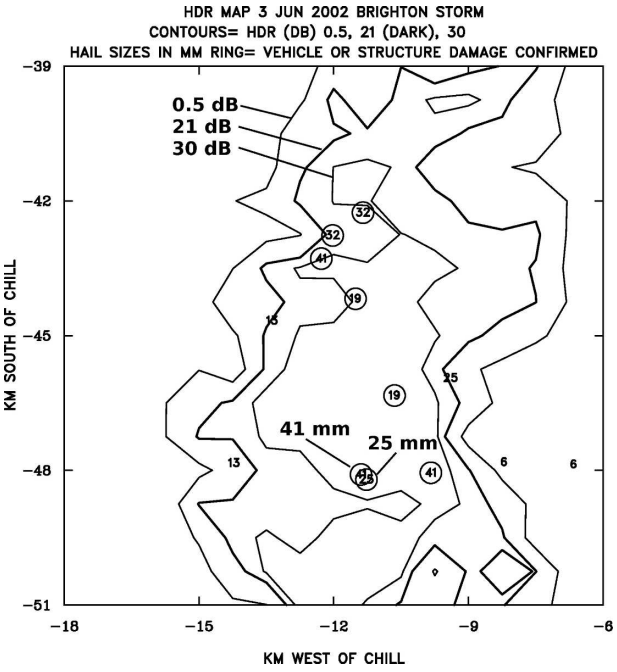

FIG. 4. Peak H_{DR} map for the 3 Jun 2002 hailstorm that occurred just northeast of Brighton, CO. Solid contours are H_{DR} (dB). Hail diameters based on poststorm interviews are marked in millimeters. Locations of observers who reported hail damage to vehicles or structures are circled.

H_{DR} value obtained at each point was retained; the resultant field is contoured in Fig. 4. The hailstone diameter and hail damage data that were collected during the poststorm surveys have been overlaid on the maximum H_{DR} contour pattern. In this case, the H_{DR} contours enclose all of the points at which larger than peasized (6-mm diameter) hail was reported. As is evident from the plot, observations of larger hail diameters and hail damage also tend to be associated with larger values of H_{DR}.

c. Scatterplots and statistical results

Figure 5 displays the reported hail diameters versus the interpolated maximum H_{DR} values derived from the radar observations for the entire dataset of 86 ground observer locations. A general correlation between H_{DR} and hail diameters can be seen, especially for hail diameters larger than ~20 mm. Points where the observers reported some manifestations of soft hail are indicated by + (not completely hard) and S (definitely soft) symbols. A number of these soft hail points are clustered in the lower right region of the scatterplot (i.e., relatively large H_{DR} values and small hail diameters). The **T**-matrix scattering calculations presented in section 2 indicate that reflectivity tends to increase

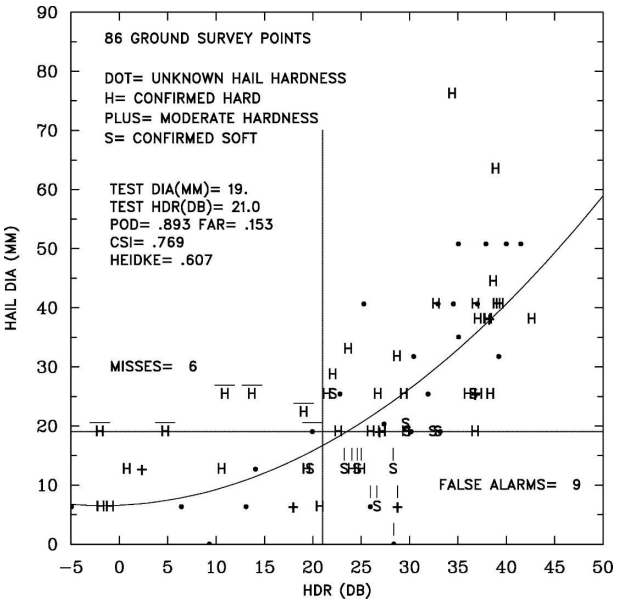

FIG. 5. Scatterplot of observer-reported hail diameters vs H_{DR}. Data point symbols indicate the observer's reports of hailstone hardness characteristics. Straight lines represent the 2×2 contingency table limits for testing the performance of a 21-dB H_{DR} threshold for the identification of hail diameters greater than or equal to 19 mm. The associated miss and false-alarm quadrants are labeled. Miss points are marked with a horizontal overbar; false-alarm points are marked with a vertical overbar. The curved line is a second-order least squares fit to the scatterplot. The standard deviation about this fit line is 10.6 mm with a correlation value (R^2) of 0.54.

by several dB when hailstones become wet and/or water-soaked, while the Z_{DR} variations remain fairly small. It appears that this reflectivity enhancement increases the H_{DR} values associated with many of the soft hail observations.

A two-by-two contingency table approach (Ryzhkov et al. 2005) was used to evaluate H_{DR} threshold values for the identification of reported hail diameters greater than or equal to 19 mm [corresponding to the National Weather Service (NWS) definition of large hail], and for the identification of structurally damaging hail. (In this study, structural damage was defined as damaged residential roofing and or building siding, broken and or cracked windows in buildings or vehicles; dented vehicle bodies, etc.) In this application, the matrix tabulations of the hits, misses, false alarms, and null events were developed for a sequence of H_{DR} threshold values. A graphical presentation of the contingency table elements is given by the intersecting straight lines included in Fig. 5. These lines depict the use of an H_{DR} threshold of 21 dB to identify hail diameter $\geq$19 mm. The H_{DR} threshold failures are indicated by the points falling within the false-alarm ($H_{DR} \geq 21$ dB, but hail diameters less than 19 mm) and miss ($H_{DR} < 21$ dB and hail diameters >19 mm) quadrants as marked in the figure. It is evident that most of the false-alarm points are associated with observations of hailstones that were reported as being less than completely hard. The use of a 21-dB H_{DR} threshold resulted in the highest critical success index (CSI; 0.77) and Heidke skill scores (HSS; 0.61) for the detection of hail with diameters of 19 mm or larger. The same reported hail-diameter database was also used to test the application of basic Z_{HH} value thresholds to identify large (>19 mm) hail. A maximum CSI value of 0.76 was obtained when a reflectivity threshold of 56 dBZ was used, and a peak Heidke score of 0.45 was obtained at 63 dBZ. The false-alarm count was found to decrease from 19 to 9 when the 21-dB H_{DR} threshold was used instead of the 56-dBZ threshold. In another analysis of reflectivity-only-based hail detection algorithms Kessinger and Brandes (1995) found that the identification of $\geq$19-mm hail typically achieved CSI values of ~0.36 and Heidke scores of ~0.42.

Additional H_{DR} threshold iterations were done to identify the threshold offering the best statistical performance for the detection of observer reports of vehicular or structural hail damage. The maximum CSI (0.78) and Heidke (0.79) scores were obtained when an H_{DR} threshold of 30 dB was tested against the reports of hail damage. Similar iterations were done to test various Z_{HH} thresholds for the detection of vehicle/structural damage. The maximum statistical index vales were a CSI of 0.67 and an HSS of 0.58, which were obtained in the 62–63-dBZ reflectivity range.

At the opposite end of the size spectrum, the H_{DR} threshold best correlated with the identification of minimal hail diameters (6 mm; pea sized) was found to occur at an H_{DR} value from -3 to -4 dB. This result was somewhat unexpected since negative H_{DR} values are conventionally associated with rain rather than hail. This statistical result was affected by two small subsets of the data; there were four cases in which the observers reported seeing 6–12-mm-diameter hail, while H_{DR} values calculated at their locations remained negative. It is possible that various rain/hail mixtures might have caused a positive Z_{DR} bias, but the observer's recollections of the precipitation characteristics in these four cases were inadequate to allow meaningful exploration of this idea. Also, there were only six rain-only (i.e., no hail, "null" observations) in the entire 86 point dataset. While these verification dataset limitations restrict statistical analysis of the basic 0-dB H_{DR} rain/hail threshold, it should be noted that the wind tunnel observations of Rasmussen et al. (1984) show that when the ice core diameter of melting hailstones becomes smaller

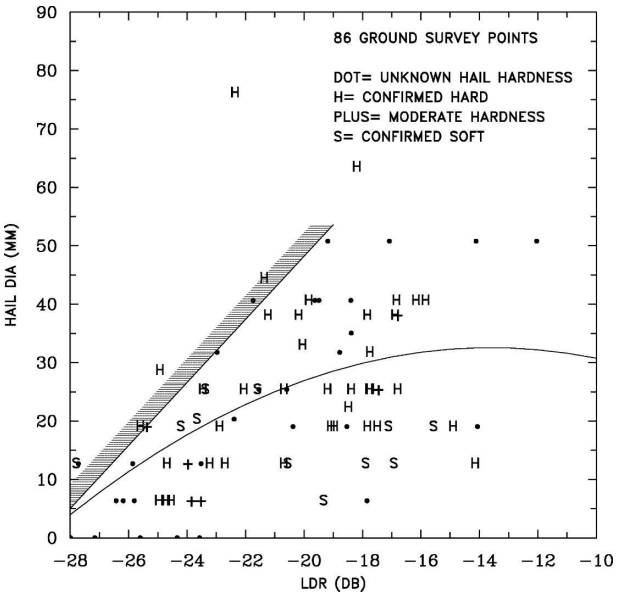

FIG. 6. Scatterplot of observer-reported hail diameters vs LDR. The feather-edged straight line is a subjective indication of the minimal LDR value associated with increasing hail diameters. Solid line is second-order polynomial least squares fit to the data points. The standard deviation about this fit line is 13 mm with a correlation value (R^2) of 0.30.

than ~9 mm, the thickening water coating can increasingly dampen the hailstone's oscillatory motions. The combination of aerodynamic forces and internal circulation patterns tend to mold this meltwater layer into an oblate shape. Thus, the Z_{DR} produced by small melting hailstones will tend to become positive. This could lead to the slightly negative H_{DR} values that were found to be associated with small hail diameters in this study.

The scatterplot of LDR and observed hail diameters is shown in Fig. 6. Significant variability is evident, with a given LDR value often being associated with a 1–3-cm range of hail diameters. Some of the points involving soft hail reports are grouped toward the higher LDR/smaller diameter region in the lower right portion of the plot domain, but many variations from this pattern are also present. A portion of this variability is probably due to nonmoisture-related factors (shape irregularities, orientation fluctuations, etc.) that also influence the LDR from hailstones.

A noteworthy aspect of the LDR versus hail diameter scatterplot is the relatively well-defined boundary that appears along the upper left limit of the data point distribution. The sloping shape of this boundary implies that the minimum LDR value associated with a given hail diameter is likely to increase with hail diameter. In other words, because of the effects of surface wetting, deviations from spherical shapes, etc., small (<19 mm in diameter) hailstones were fairly commonly observed to be associated with relatively large (>~−22 dB) LDR values. However, distinctly large hail diameters (>~30 mm) were rarely associated with LDR levels of less than approximately −24 dB. Thus, while the observed LDR magnitudes alone did not provide much hail size information, the absence of relatively low LDR values within a hail area may indicate an increased probability that large hail is present.

d. An example of H_{DR} and LDR time evolution

As described earlier, the data shown in the scatterplots were collected at the time when H_{DR} values maximized as a hailstorm passed a given ground observer location. Additional information can be obtained by considering the evolution of the polarimetric radar measurements over the time period included in a sequence of volume scans. For this purpose, the high time-resolution data collected by the CSU-CHILL radar during the afternoon of 9 June 2004 were processed. In this radar operation, low-elevation angle PPI sector scans were being done with a nominal cycle time of two min during the National Aeronautics and Space Administration (NASA)-supported Front Range Pilot Project in preparation for the future Global Precipitation Measurement satellite mission (Rutledge et al. 2005). The storm of interest passed over a golf course located in southern Denver where witnesses noted how the hail characteristics varied with time. During the initial stages of the event, the ground became covered with hailstones whose average size was approximately 12.5 mm; only a small fraction of the stones were of appreciably larger diameters. Following a brief reduction in precipitation intensity, a second, noticeably more vigorous episode of larger diameter hail occurred. Significant damage to buildings, vehicles, and the golf course turf was observed to occur during the second hail pulse. Maximum hail diameters of 30–40 mm were frequently observed during the second hail episode.

Time histories of selected CSU-CHILL radar measurements over the golf course location are shown in Fig. 7. The data plotted in these traces are based on the 0.5° elevation sweep in each PPI volume scan. In each of these sweeps, data from the six range gates that surrounded the golf course location (i.e., the three closest range gates in the two rays located on either side of the golf course azimuth) were extracted. Representative radar data values at the golf course location were developed by first applying a basic triangular weighting scheme in range and then interpolating in azimuth between the two flanking rays.

Reflectivities generally increased between 2015 and 2030 UTC. During this same period, the Z_{DR} values

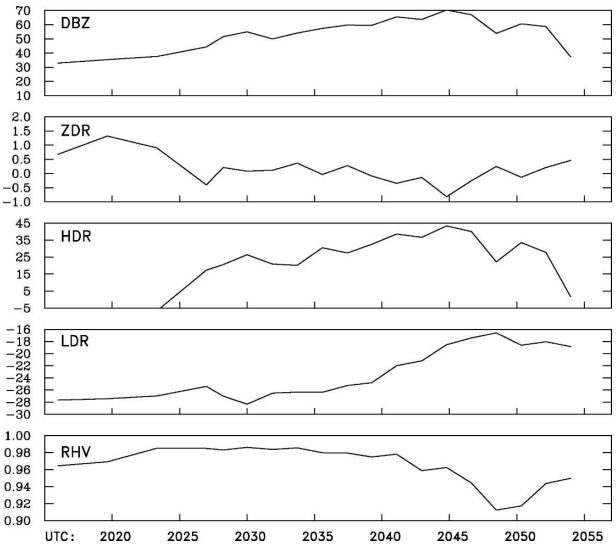

FIG. 7. Time series of CSU-CHILL data from a sequence of 0.5° PPI sweeps on 9 Jun 2004 interpolated to the Foothills Golf Course in southeast Denver, CO. UTC times (HHMM, where H is hours and M is minutes) are marked at 5-min intervals.

initially became more positive, but then decreased toward 0 dB as the first period of hail developed (H_{DR} first reached +5 dB at ~2025 UTC). The LDRs fluctuated, but remained below approximately −25 dB throughout this period. Following a brief decline in reflectivity around 2033 UTC, the storm began to build toward its second intensity peak in which reflectivities approached 70 dBZ at 2045 UTC. The Z_{DR} values decreased during this intensification and became slightly negative between ~2040 and 2048 UTC. These diverging dBZ and Z_{DR} trends resulted in large positive (from 25 to >40 dB) H_{DR} values during the second (damaging) hail episode. It is noteworthy that the minimum Z_{DR} values became slightly negative; there is observational evidence (Husson and Pointin 1989) relating the simultaneous occurrence of large Z_{HH} and negative Z_{DR} to damaging hail. The onset of this period of hail was also characterized by a significant LDR increase, with the peak depolarization levels exceeding −18 dB just before 2050 UTC. These time variations of the polarimetric radar data fields in relationship to the surface observations of large hail are consistent with those reported by Hubbert et al. (1998, their Fig. 11). It is apparent in this case that both the H_{DR} and LDR values increased appreciably during the later portion of the storm's passage when larger-diameter, structurally damaging hail fell.

Although not otherwise analyzed in this study, a time history of the correlation between the H and V signal returns corrected for the interpulse time period between H and V transmissions [$\rho_{HV}(0)$] is shown in Fig. 7e. The $\rho_{HV}(0)$ values maximize when distributions of the sizes, shapes, and orientations of the hydrometeors in the pulse volume are narrow. Balakrishnan and Zrnic (1990) report that in pure rain observed at S band (i.e., negligible Mie scattering effects), [$\rho_{HV}(0)$] is typically ~0.98. Mixtures of rain and hail within the pulse volume can lower $\rho_{HV}(0)$ magnitudes to ~0.90 or less; the occurrence of high values of Z_{HH} in combination with low Z_{DR} and $\rho_{HV}(0)$ has been found to provide an indication of hail (Ryzhkov et al. 2005). This behavior is evident in Fig. 7 when, in agreement with the other radar measurements, a $\rho_{HV}(0)$ drop to ~0.91 took place during the damaging hail phase toward the end of the storm passage at the golf course. The $\rho_{HV}(0)$ minimum occurred several minutes after the ZDR minimum. This may indicate that the rain–hail proportions became the most effective in reducing $\rho_{HV}(0)$ at ~2049 UTC. In general, $\rho_{HV}(0)$ provides additional hail characterization information that is especially useful for polarimetric radars that operate with simultaneous H and V transmission schemes that prevent the direct measurement of LDR (Doviak et al. 2000; Heinselman and Rowe 2005; Heinselman and Ryzhkov 2006).

Histograms of the LDR values at 2033 and 2045 UTC are shown in Fig. 8. The gate data plotted in these histograms came from a 4 km × 4 km region centered on the golf course location. Additionally, all of the gates used in the histograms were required to have a minimum H_{DR} of 0 dB. Thus, they represent the distribution of LDR values within the H_{DR}-identified hail areas during the nondamaging (2033 UTC) and severe hail (2044 UTC) hail episodes. A positive shift of several dB is evident in the LDR distribution that was associated with the large hail. Also, in agreement with the pattern noted in Fig. 6, the occurrence of relatively low (<~−24 dB) LDR values was rare when large hail was occurring in the 4 km × 4 km domain that provided the histogram data.

4. Conclusions

The results of this study indicate that the magnitude of the H_{DR} parameter as originally formulated by Aydin et al. (1986) provides useful, quantitative information for remotely sensing some important hail characteristics. In particular, the existence of hail sizes commensurate with the NWS definition of large hail (19 mm diameter) is likely when H_{DR} reaches 21 dB. Reports of hail damage to residential structures and vehicles were observed to be associated with H_{DR} >30 dB. These thresholds help refine the basic correlation between H_{DR} magnitude and hail size noted by Brandes and Vivekanandan (1998). False identifications of large hail by H_{DR} tend to be associated with

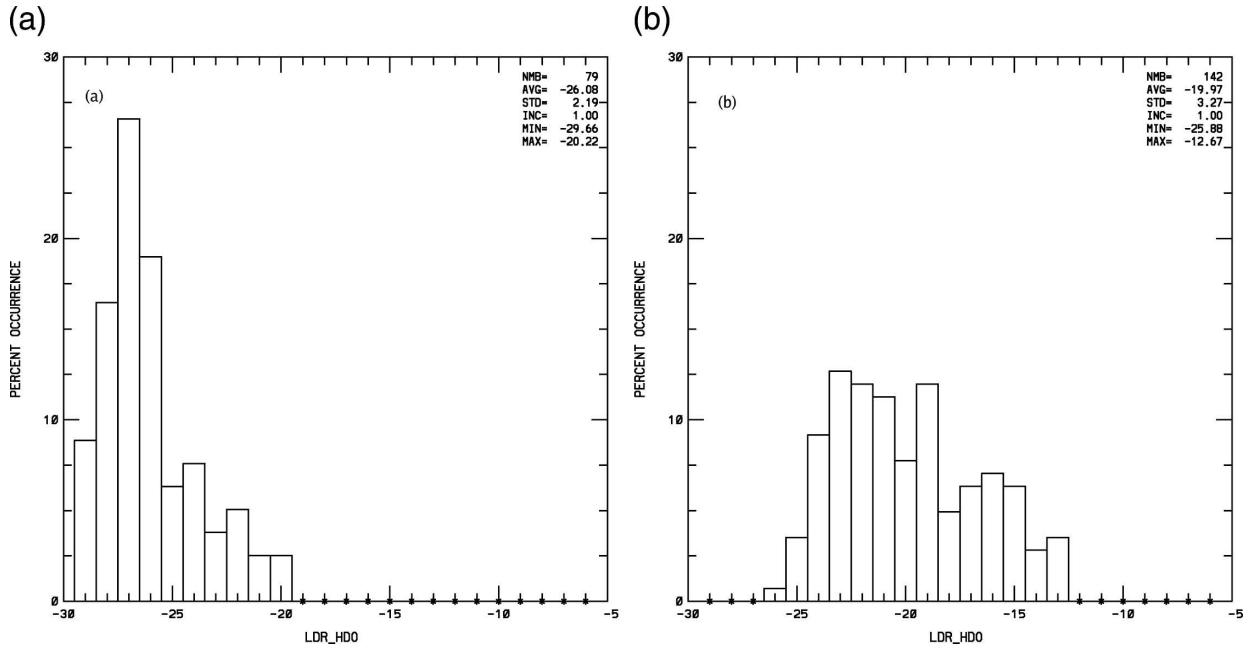

FIG. 8. LDR histograms from the range gates within a 4-km-square box centered on the location where the traces in Fig. 7 were extracted. Input data are from the 0.5° elevation PPI sweeps. Only gates with H_{DR} values of 0 dB or greater (i.e., containing hail) are included in the histograms; (a) 2033 and (b) 2045 UTC.

observations of soft, presumably wetter, hailstones. The **T**-matrix scattering model calculations indicate that these H_{DR} false alarms may be due to the several-decibel reflectivity increases that often develop when hailstones become water-soaked. Overall, as measured by the critical success index and Heidke skill scores, the ability of the proposed H_{DR} thresholds for the identification of large and damaging hail is superior to the statistical performance levels achieved by techniques using only conventional, single-polarization radar data.

In contrast, the linear depolarization ratio levels interpolated to the ground-observer locations were found to have only limited correlation with the observed hail sizes. Qualitatively, larger LDR values will be produced by the less spherical shapes and more irregular surface features that are often present in larger diameter hailstones. However, the backscattering calculations done in this study and elsewhere (Aydin and Zhao 1990) show that LDR is also significantly affected by variations in the bulk ice density and liquid water content (both within the ice structure and on the outer surface) of the hailstones. Thus, the basic LDR–hail diameter correlation is indistinct. While small hailstones can sometimes generate fairly large LDR levels, the ground-truth observations in this study indicate that the occurrence of low ($<\sim -25$ dB) LDR levels becomes rare when hail diameters exceed 25 to 30 mm. Thus, the general absence of these low LDR values within a highly positive H_{DR} region may help to confirm the basic implication that large hail is present.

This study indicates that the H_{DR} parameter has useful hail characterization capabilities (at least in the general Colorado High Plains region). These results should be verified in other precipitation regimes. If the H_{DR} thresholds suggested in this work are valid, they may also provide reference points for the evaluation of more elaborate fuzzy logic (Liu and Chandrasekar 2000) hail identification and categorization algorithms.

Acknowledgments. The CSU-CHILL Radar Facility is supported by the National Science Foundation (NSF) cooperative agreement ATM-0118021 and Colorado State University. Most of the CSU-CHILL radar data collected for this study were a part of the UCAR COMET Grant S02-38660. The Front Range Pilot Project was supported by NASA Grants NAG5-13623 and NNG04GF32A. We also thank David Brunkow and Robert Bowie of the CHILL Radar Facility for their assistance with radar operations. The anonymous reviewers of the original manuscript also provided several useful improvements to the paper.

REFERENCES

Aydin, K., and Y. Zhao, 1990: A computational study of polarimetric radar observables in hail. *IEEE Trans. Geosci. Remote Sens.,* **28,** 412–422.

——, T. A. Seliga, and V. Balaji, 1986: Remote sensing of hail with a dual-linear polarization radar. *J. Climate Appl. Meteor.,* **25,** 1475–1484.

Balakrishnan, N., and D. S. Zrnic, 1990: Use of polarization to characterize precipitation and discriminate large hail. *J. Atmos. Sci.,* **47,** 1525–1540.

Beard, K. V., and C. Chuang, 1987: A new model for the equilibrium shape of raindrops. *J. Atmos. Sci.,* **44,** 1509–1524.

Brandes, E. A., and J. Vivekanandan, 1998: An exploratory study in hail detection with polarimetric radar. Preprints, *14th Conf. on Interactive Information and Processing Systems for Meteorology, Oceanography and Hydrology,* Phoenix, AZ, Amer. Meteor. Soc., 287–290.

Brunkow, D., V. N. Bringi, P. C. Kennedy, S. A. Rutledge, V. Chandrasekar, E. A. Mueller, and R. K. Bowie, 2000: A description of the CSU-CHILL national radar facility. *J. Atmos. Oceanic Technol.,* **17,** 1596–1608.

Cheng, L., and M. English, 1983: A relationship between hailstone concentration and size. *J. Atmos. Sci.,* **40,** 204–213.

Cressman, G. P., 1959: An operational objective analysis scheme. *Mon. Wea. Rev.,* **87,** 367–374.

Doviak, R. J., V. Bringi, A. Ryzhkov, A. Zahrai, and D. Zrnić, 2000: Considerations for polarimetric upgrades to operational WSR-88D radars. *J. Atmos. Oceanic Technol.,* **17,** 257–278.

Heinselman, P. A., and A. Rowe, 2005: Estimating hail size using polarimetric radar. Preprints, *32d Conf. on Radar Meteorology,* Albuquerque, NM, Amer. Meteor. Soc., CD-ROM, P1.45.

——, and A. V. Ryzhkov, 2006: Validation of polarimetric hail detection. *Wea. Forecasting,* **21,** 839–850.

Herzegh, P. H., and A. R. Jameson, 1992: Observing precipitation through dual-polarization radar. *Bull. Amer. Meteor. Soc.,* **73,** 1365–1374.

Hubbert, J., V. N. Bringi, L. D. Carey, and S. Bolen, 1998: CSU-CHILL polarimetric radar measurements from a severe hail storm in eastern Colorado. *J. Appl. Meteor.,* **37,** 749–775.

Husson, D., and Y. Pointin, 1989: Quantative estimation of the hailfall intensity with dual polarization radar and a hailpad network. Preprints, *24th Conf. on Radar Meteorology,* Tallahassee, FL, Amer. Meteor. Soc., 318–321.

Kessinger, C. J., and E. A. Brandes, 1995: A comparison of hail detection algorithms. Project Summary Rep., National Center for Atmospheric Research, 52 pp.

Knight, C. A., and N. C. Knight, 1970a: Lobe structures of hailstones. *J. Atmos. Sci.,* **27,** 667–671.

——, and ——, 1970b: The falling behavior of hailstones. *J. Atmos. Sci.,* **27,** 672–681.

Knight, N. C., 1986: Hailstone shape factor and its relationship to radar interpretation of hail. *J. Climate Appl. Meteor.,* **25,** 1956–1958.

Liu, H., and V. Chandrasekar, 2000: Classification of hydrometeors based on polarimetric radar measurements: Development of fuzzy logic and neuro-fuzzy systems, and in situ verification. *J. Atmos. Oceanic Technol.,* **17,** 140–164.

Mezzasalma, P., S. Nanni, and P. P. Alberoni, 2000: Performance of a Hdr-based hail detection algorithm in Northern Italy. *Phys. Chem. Earth,* **25B,** 949–952.

Pruppacher, H. R., and K. V. Beard, 1970: A wind tunnel investigation of the internal circulation and shape of water drops falling at terminal velocity in air. *Quart. J. Roy. Meteor. Soc.,* **96,** 247–256.

Rasmussen, R. M., and A. J. Heymsfield, 1987: Melting and shedding of graupel and hail. Part II: Sensitivity study. *J. Atmos. Sci.,* **44,** 2764–2782.

——, V. Levizzani, and H. R. Pruppacher, 1984: A wind tunnel and theoretical study on the melting behavior of atmospheric ice particles. Part III. Experiment and theory for spherical ice particles of radius >500 μm. *J. Atmos. Sci.,* **41,** 381–388.

Rutledge, S. A., and Coauthors, 2005: The Front Range pilot project for GPM: An instrument and concept test. Preprints, *32d Conf. on Radar Meteorology,* Albuquerque, NM, Amer. Meteor. Soc., CD-ROM, P6R.2

Ryzhkov, A. V., T. J. Schuur, D. W. Burgess, P. Heinselman, S. E. Giangrande, and D. S. Zrnic, 2005: The joint polarization experiment. *Bull. Amer. Meteor. Soc.,* **86,** 809–824.

Seliga, T. A., and V. N. Bringi, 1976: Potential use of radar differential reflectivity measurements at orthogonal polarizations for measuring precipitation. *J. Appl. Meteor.,* **15,** 69–76.

Smyth, T. J., T. M. Blackman, and A. J. Illingworth, 1999: Observations of oblate hail using dual polarization radar and implications for hail-detection schemes. *Quart. J. Roy. Meteor. Soc.,* **125,** 993–1016.

Ulbrich, C. W., and D. Atlas, 1982: Hail parameters: A comprehensive digest. *J. Appl. Meteor.,* **21,** 22–43.

Waterman, P. C., 1965: Matrix formulation of electromagnetic scattering. *Proc. IEEE,* **53,** 805–812.